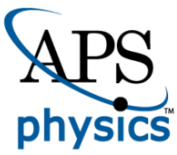

Does Flexoelectricity Drive Triboelectricity?

C. A. Mizzi, A. Y. W. Lin, and L. D. Marks

Phys. Rev. Lett. **123**, 116103 — Published 12 September 2019

DOI: 10.1103/PhysRevLett.123.116103

Does Flexoelectricity Drive Triboelectricity?

C. A. Mizzi*, A. Y. W. Lin* and L. D. Marks[1]
Department of Materials Science and Engineering
Northwestern University, Evanston, IL 60208

*These authors contributed equally to this work

Corresponding Author

[1]To whom correspondence should be addressed. Email: L-marks@northwestern.edu.

Abstract

The triboelectric effect, charge transfer during sliding, is well established but the thermodynamic driver is not well understood. We hypothesize here that flexoelectric potential differences induced by inhomogeneous strains at nanoscale asperities drive tribocharge separation. Modelling single asperity elastic contacts suggests that nanoscale flexoelectric potential differences of ±1-10 V or larger arise during indentation and pull-off. This hypothesis agrees with several experimental observations, including bipolar charging during stick-slip, inhomogeneous tribocharge patterns, charging between similar materials, and surface charge density measurements.

The triboelectric effect, the transfer of charge associated with rubbing or contacting two materials, has been known for at least twenty-five centuries [1,2]. The consequences of this transfer are known to be beneficial and detrimental; for instance, tribocharging is widely exploited in technologies such as laser printers but can also cause electrostatic discharges that lead to fires. It is accepted that it involves the transfer of charged species, either electrons [3-5], ions [6,7], or charged molecular fragments [8], between two materials. The nature and identification of these charged species has been the focus of considerable research [2,9], but an important unresolved issue is the thermodynamic driver for charge transfer; the process of separating and transferring charge must reduce the free energy of the system. What is the charge transfer driver? In some cases specific drivers are well understood. For instance, when two metals with different work functions are brought into contact charge transfer will occur until the chemical potential of the electrons (Fermi level) is the same everywhere. Triboelectric charge transfer in insulators is less understood; proposed models include local heating [10] and trapped charge tunneling [11-13] but these models do not explicitly address the significant mechanical deformations associated with bringing two materials into contact and rubbing them together. Furthermore there is currently little ab-initio or direct numerical connection between experimental measurements and proposed drivers.

Since the pioneering work of Bowden and Tabor [14] it has been known that friction and wear at the nanoscale is associated with adhesion between, as well as the elastic and plastic deformation of, a statistical population of asperities. It is also well established that elastic deformation is thermodynamically linked to polarization: the linear coupling between strain and polarization is the piezoelectric effect and the linear coupling between strain gradient and polarization is the flexoelectric effect [15-17]. While piezoelectric contributions only occur for

materials without an inversion center, flexoelectric contributions occur in all insulators and can be large at the nanoscale due to the intrinsic size scaling of strain gradients [17-19]. Quite a few papers have analyzed the implications of these coupling terms in phenomena including nanoindentation [20,21], fracture [22], and tunneling [23]. There also exists literature where the consequences of charging on friction have been studied [24-26], and frictional properties have been related to redistributions of interfacial charge density via first principles calculations [27]. However, triboelectricity, flexoelectricity, and friction during sliding are typically considered as three independent phenomena.

Are they really uncoupled phenomena? In this paper we hypothesize that the electric fields induced by inhomogeneous deformations at asperities via the flexoelectric effect lead to significant surface potentials differences, which can act as the driver for triboelectric charge separation and transfer. The flexoelectric effect may therefore be a very significant, and perhaps even the dominant, thermodynamic driver underlying triboelectric phenomena in many cases. To investigate this hypothesis in detail we analyze, within the conventional Hertzian [28] and Johnson-Kendall-Roberts (JKR) [29] contact models, the typical surface potential differences around an asperity in contact with a surface during indentation and pull-off. We find that surface potential differences in the range of ±1-10 V or more can be readily induced for typical polymers and ceramics at the nanoscale, and that the intrinsic asymmetry of the inhomogeneous strains during indentation and pull-off changes the sign of the surface potential difference. We argue that our model is consistent with a range of experimental observations, in particular bipolar tribocurrents associated with stick-slip [30], the scaling of tribocurrent with indentation force [31], the phenomenon of tribocharging of similar materials [32-35], and the inhomogeneous charging of insulators [36,37]. Taking the analysis a step further, our model suggests a suitable

upper bound for the triboelectric surface charge density is the flexoelectric polarization that is found to be in semi-quantitative agreement with published experimental data without the need to invoke any empirical parameters. Given the recent ab-initio developments of flexoelectric theory [38-41], we argue that flexoelectricity can provide an ab-initio understanding of many triboelectric phenomena.

Nanoscale asperity contact consists of two main phenomena, indentation and pull-off, which are illustrated in Fig. 1. To investigate the electric fields arising from the strain gradients associated with these two processes, we combine the constitutive flexoelectric equations with the classic Hertzian and JKR models, for simplicity considering only vertical relative displacements; see later for some comments about shear. As discussed further in the Supplemental Material [57], the normal component of the electric field induced by a flexoelectric coupling in an isotropic non-piezoelectric half plane oriented normal to $\hat{z}$ is given by:

$$E_z = -f\left.\frac{\partial \epsilon}{\partial z}\right|_{eff} = -f\left(3\epsilon_{zzz} + \epsilon_{zxx} + \epsilon_{xzx} + \epsilon_{xxz} + \epsilon_{zyy} + \epsilon_{yzy} + \epsilon_{yyz}\right) \quad (1)$$

where E_z is the electric field linearly induced by $\left.\frac{\partial \epsilon}{\partial z}\right|_{eff}$ the effective strain gradient. The proportionality constant f is the flexocoupling voltage (i.e., the flexoelectric coefficient divided by the dielectric constant) and the effective strain gradient is the sum of the symmetry-allowed strain gradient components (where $\epsilon_{jkl} = \frac{\partial \epsilon_{jk}}{\partial x_l}$).

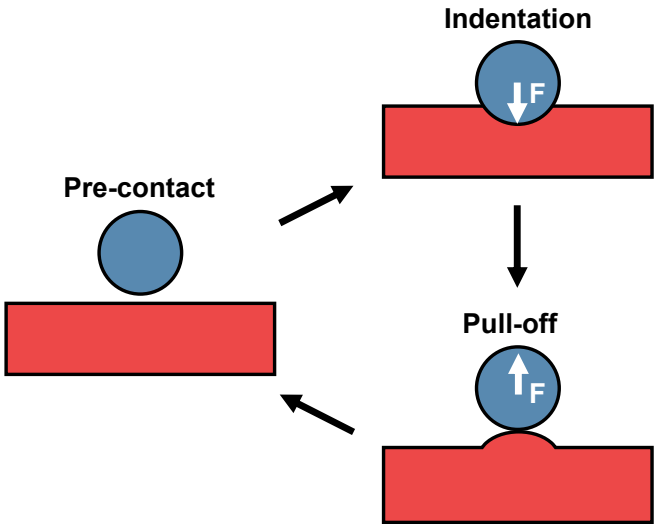

Fig. 1. Schematic of asperity contact between a rigid sphere (blue) and an elastic body (red). During indentation and pull-off the elastic body will deform, developing a net strain gradient opposite to the direction of the applied force (F).

First, we will analyze the indentation case. Because of the axial symmetry of Hertzian indentation, only five strain gradient components in Equation (1) are symmetrically inequivalent. Expressions for these components are derived from classic Hertzian stresses (see Supplemental Material [57]) and depicted in Fig. 2(a)-(e) as contour plots. From these plots it is evident that the strain gradient components have complex spatial distributions, the details of which depend on the materials properties of the deformed body (Young's modulus, Poisson's ratio) as well as external parameters (applied force, indenter size). Further insight can be gained by calculating the average effective strain gradient within the indentation volume, which is taken to be the cube of the deformation radius. The average effective strain gradient is negative and scales inversely with indenter size, independent of the materials properties of the deformed body and the applied force. The former is intuitive since a material deformed by an indenter should develop a curvature opposite to the direction of the applied force, and the latter is a consequence of averaging (Supplemental Material [57]). As shown in Fig. 2(f), the average effective strain

gradient associated with Hertzian indentation is on the order of -10^8 m^{-1} in all materials at the nanoscale. Such large strain gradients immediately suggest the importance of flexoelectric couplings [17,18].

For pull-off we use JKR theory, which incorporates adhesion effects between a spherical indenter and an elastic half-space into the Hertz contact model. The tensile force required to separate the indenter from the surface, also known as the pull-off force, can be written as

$$F_{adh} = -\frac{3}{2}\pi \Delta\gamma R \qquad (2)$$

where $\Delta\gamma$ is the adhesive energy per unit area and R is the radius of the spherical indenter. Replacing the applied force in the Hertzian indentation strain gradient expressions with this force yields pull-off strain gradients immediately before contact is broken. This analysis for the pull-off case yields strain gradient distributions qualitatively similar to those shown in Fig. 2, except with opposite signs because the force is applied in the opposite direction. Importantly, as in the indentation case, the average effective strain gradient within the pull-off volume scales inversely with indenter size, is independent of the materials properties of the deformed body, and is on the order of 10^8 m^{-1} in all materials at the nanoscale.

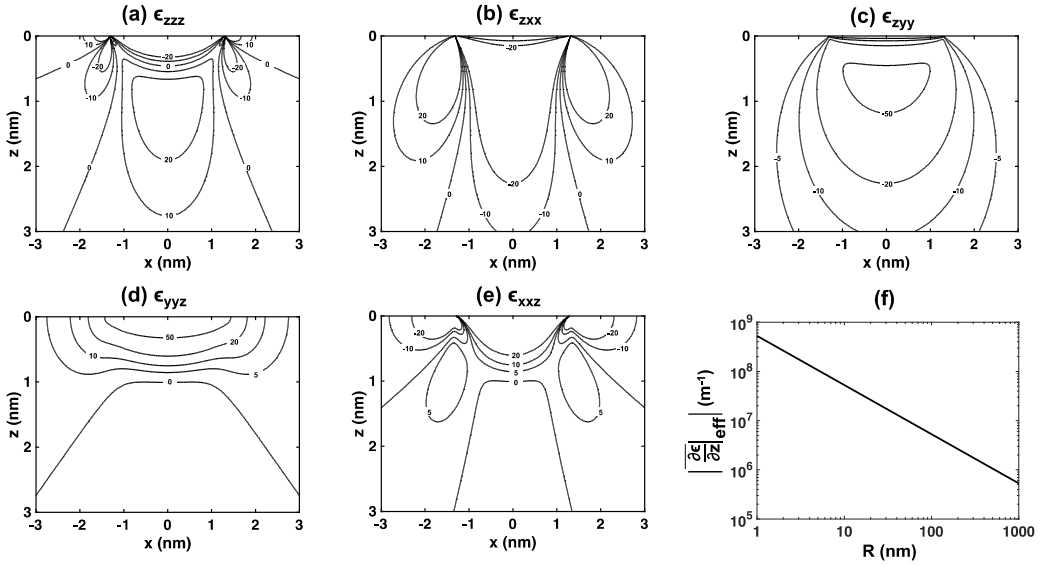

Fig. 2. (a) – (e) Symmetrically inequivalent strain gradients arising from Hertzian indentation of an elastic half-space that can flexoelectrically couple to the normal component of the electric field. Lines indicate constant strain gradient contours in units of 10^6 m^{-1}, z is the direction normal to the surface with positive values going into the bulk, x is an in-plane direction, and the origin is the central point of contact. Data corresponds to 1 nN of force (a conservatively small number) applied to an elastic half-space with a Young's modulus of 3 GPa and a Poisson's ratio of 0.3 (typical polymer) by a 10 nm rigid indenter. (f) The magnitude of the average effective strain gradient ($\left|\overline{\frac{\partial \epsilon}{\partial z}}\right|_{eff}$) as a function of indenter radius (R). The average effective strain gradient corresponds to a sum of the strain gradient components shown in (a) – (e) averaged over the indentation/pull-off volumes.

We now turn to the flexoelectric response to these deformations. Obtaining analytical expressions for the normal component of the electric field in the deformed body induced by indentation and pull-off involves substituting the strain gradient components shown in Fig. 2 into Equation (1). This electric field component is shown in Fig. 3 for the indentation case with a positive flexocoupling voltage. The pull-off case is similar, but the signs of the electric fields are reversed. Because the electric field induced by the flexoelectric effect is the effective strain gradient scaled by the flexocoupling voltage, its magnitude is linearly proportional to the flexocoupling voltage and inversely proportional to the indenter size. The average electric field in the indentation/pull-off volume is on the order of 10^8-10^9 V/m for all materials at the nanoscale assuming a conservative flexocoupling voltage of 1 V [16,17,42]; some specific flexocoupling voltages are given in Supplemental Tables S1 and S2 [57].

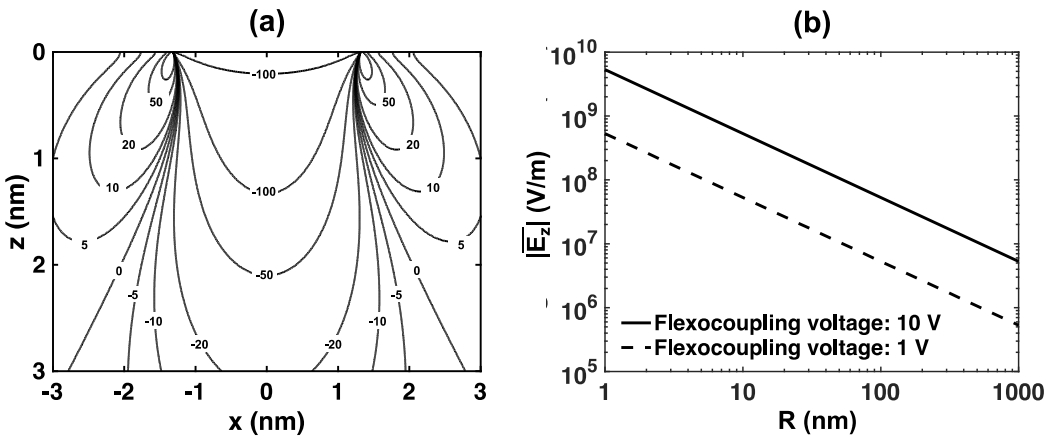

Fig. 3. (a) Normal component of the electric field induced by Hertzian indentation via a flexoelectric coupling. Lines indicate constant electric field contours in units of MV/m, z is the direction normal to the surface with positive values going into the bulk, x is an in-plane direction, and the origin is the central point of contact. Data corresponds to 1 nN of force applied to an elastic half-space with a Young's modulus of 3 GPa and a Poisson's ratio of 0.3 (typical polymer) by a 10 nm indenter. A flexocoupling voltage of 1 V is assumed. (b) Magnitude of the average electric field ($|\overline{E_z}|$) in the indentation/pull-off volumes as a function of indenter radius (R) assuming a flexocoupling voltage of 1 V (dashed) and 10 V (solid).

The electric fields induced by the flexoelectric effect in the bulk of the deformed body will generate a potential on its surface. Figure 4 depicts the surface potential difference calculated from the normal component of the electric field (Supplemental Material [57]) along the deformed surface of a typical polymer with a flexocoupling voltage of 10 V [16,17,42]; the available measured flexocoupling voltages for polymers indicates that this may be a significant underestimate, see Supplemental Table S2 [57]. The pull-off surface potential difference tends to be larger in magnitude and spatial extent than the indentation surface potential difference. In both cases the magnitude of the maximum surface potential difference is sensitive to the materials properties of the deformed body (Young's modulus, Poisson's ratio, adhesion energy, flexocoupling voltage) and external parameters (applied force, indenter size). Specifically, the surface potential differences for indentation and pull-off scale as

— (3)

— (4)

where is the minimum surface potential difference for indentation, is the maximum surface potential difference for pull-off, is the flexocoupling voltage, is the applied force, is the indenter radius, is the Young's modulus, and is the energy of adhesion.

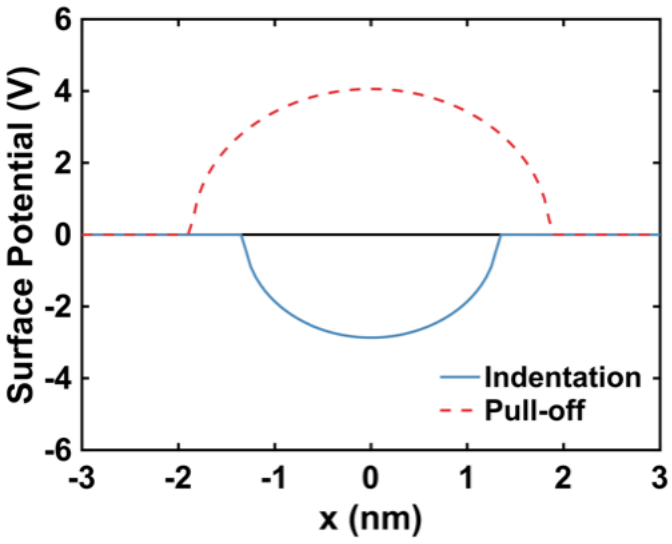

Fig. 4. Electric potential difference along the surface of the deformed body for indentation (solid) and pull-off (dashed). is an in-plane direction and the origin is the central point of contact. Data corresponds to 1 nN of force applied to an elastic half-space with a Young's modulus of 3 GPa, a Poisson's ratio of 0.3, adhesion energy of 0.06 N/m (typical polymer), and flexocoupling voltage of 10 V by a 10 nm indenter.

The above analysis indicates that large strain gradients arising from deformations by nanoscale asperities yield surface potential differences via a flexoelectric coupling in the ±1-10 V range, as a conservative estimate. The magnitude of this surface potential difference is sufficient to drive charge transfer, suggesting that flexoelectric couplings during indentation and pull-off can be responsible for triboelectric charging. Furthermore, this model implies that the

direction of charge transfer is controlled by a combination of the direction of the applied force and local topography (i.e. is the asperity indenting or pulling-off), as well as the sign of the flexocoupling voltage.

These features are consistent with and can explain a significant number of previous triboelectric observations without introducing any adjustable parameters. First, it has been observed that tribocurrents exhibit bipolar characteristics associated with stick-slip [30]. This bipolar nature is consistent with the change in the sign of the surface potential difference for indentation and pull-off predicted by our model. We note that these experiments had some shear component which is not exactly the same as our analysis and complicates the problem due to the breakdown of circular symmetry. While this will yield a more complex strain gradient distribution than our simplified model, the total potential difference will be the sum of normal and shear contributions which does not change our general conclusions. Second, the tribocurrent has been shown to scale with the indentation force to the power of $\frac{1}{3}$ [31], which matches the scaling of the indentation surface potential difference with force. Thirdly, charging between similar materials [32-35] and the formation of non-uniform tribocharge patterns [36,37,43,44] can be explained by considering the effect of local surface topography and crystallography on the direction of charge transfer: local variation in surface topography dictates which material locally acts as the asperity, and consequently the direction in which charge transfers. In addition, it is established for crystalline materials that both the magnitude and sign of the flexocoupling voltage can change with crystallographic orientation (Supplemental Table S1 [57]). Finally, recent work has demonstrated that macroscopic curvature biases tribocharging so that convex samples tend to charge negative and concave samples tend to charge positive; this coupling

between curvature and charge transfer direction is a natural consequence of our flexoelectric model [45].

Going beyond these qualitative conclusions, it is relevant to explore whether flexoelectricity can quantitatively explain experimental triboelectric charge transfer measurements. An important quantitative parameter in the triboelectric literature is the magnitude of triboelectric surface charge density which has been measured in a number of systems including spherical particles [35,46] and patterned triboelectric devices [47,48], and normally enters models as an empirical parameter [49,50]. We hypothesize that the upper bound for the triboelectric surface charge density is set by the flexoelectric polarization, i.e. charge will transfer until the flexoelectric polarization is screened (Supplemental Material [57]). As shown in Table 1, this hypothesis agrees with existing tribocharge measurements on a range of length scales to within an order of magnitude without invoking anomalous flexoelectric coefficients.

Reference	**Feature Size**	**σ_{tribo} ($\mu C/m^2$)**	**P_{FxE}($\mu C/m^2$)**
[46]	2.8 mm	0.5	0.4
[35]	326 μm	0.2	1.6
[35]	251μm	0.5	2.1
[47,48]	10 μm	97.4	106.1

Table 1. Comparison between measured triboelectric surface charge (σ_{tribo}) and calculated flexoelectric polarization (P_{FxE}) for feature sizes in the mm to μm range assuming a flexoelectric coefficient of 1 nC/m.

These results make a strong case that the flexoelectric effect drives triboelectric charge separation and transfer, and that nanoscale friction, flexoelectricity, and triboelectricity occur simultaneously and are intimately linked: macroscopic forces during sliding on insulators cause local inhomogeneous strains at contacting asperities which induce significant local electric fields

which in turn drive charge separation. This analysis does not depend upon the details of the charge species, they may be electrons, polymeric ions, charged point defects in oxides, or some combination. Hence our model does not contradict any of the existing literature on the nature of the charge species, instead it provides a thermodynamic rationale for the charge separation to occur. We have deliberately used very conservative numbers for the flexocoupling voltage, and many materials are known to have significantly larger values – see Supplemental Tables S1 and S2 [57]. It is therefore very plausible that much larger potential differences can be generated. Our analysis also suggests ways to optimize charge separation (e.g. assuming pull-off dominates, based upon Equation (4) one wants a relatively soft material with a high flexocoupling voltage, large adhesion, and many small asperities). Some additional experimental and theoretical ways to assess this model are discussed briefly in the Supplemental Material [57].

In addition, the formalism we have used is not limited to inorganic materials, but is quite general. As one extension it is known that semi-crystalline layers are formed at the confined spaces during sliding in a lubricant [51], so it is not unreasonable that flexoelectric effects can drive charge separation in lubricants. Another extension is biological materials, as flexoelectric effects in biological membranes are well-established [52]. We also note the magnitude of the flexoelectricity-induced electric fields and surface potential differences at asperities (and crack tips [22]) suggest flexoelectricity can play a role in triboluminescence [53-55], triboplasma generation [56] or tribochemical reactions. Such hypotheses merit further work.

In summary, using the Hertz and JKR models for indentation and pull-off, we show that deformations by nanoscale asperities yield surface potential differences via a flexoelectric coupling in the ±1-10 V range or more, large enough to drive charge separation and transfer. The direction and magnitude of the surface potential differences depend on the applied force, asperity

size, local topography, and material properties. These findings explain some previous tribocharging observations and we argue are the first steps towards an ab-initio understanding of triboelectric phenomena.

Acknowledgements: This work was supported by the National Science Foundation Grant No. CMMI-1400618 (AYWL) and the U.S. Department of Energy, Office of Science, Basic Energy Sciences, under Award No. DE-FG02-01ER45945 (CAM).

Author Contributions: CAM and AYWL performed the analysis supervised by LDM. All authors contributed to the writing of the Letter.

References

[1] W. R. Harper, *Contact and Frictional Electrification* (Oxford University Press, Oxford, 1967).

[2] D. J. Lacks and R. M. Sankaran, Journal of Physics D: Applied Physics **44**, 453001 (2011).

[3] C. Y. Liu and A. J. Bard, Nature Materials **7**, 505 (2008).

[4] J. Lowell and A. C. Rose-Innes, Advances in Physics **29**, 947 (2006).

[5] D. K. Davies, Journal of Physics D: Applied Physics **2**, 1533 (1969).

[6] A. F. Diaz and D. Fenzel-Alexander, Langmuir **9**, 1009 (1993).

[7] L. S. McCarty and G. M. Whitesides, Angew Chem Int Ed Engl **47**, 2188 (2008).

[8] H. T. Baytekin, B. Baytekin, J. T. Incorvati, and B. A. Grzybowski, Angew Chem Int Ed Engl **51**, 4843 (2012).

[9] F. Galembeck, T. A. L. Burgo, L. B. S. Balestrin, R. F. Gouveia, C. A. Silva, and A. Galembeck, RSC Advances **4**, 64280 (2014).

[10] S. Lin *et al.*, Advanced Materials, 1808197 (2019).

[11] J. F. Kok and D. J. Lacks, Physical Review E **79**, 051304 (2009).

[12] D. J. Lacks, N. Duff, and S. K. Kumar, Physical Review Letters **100**, 188305 (2008).

[13] J. Lowell and W. S. Truscott, Journal of Applied Physics D: Applied Physics **19** (1986).

[14] F. P. Bowden and D. Tabor, *The Friction and Lubrication of Solids* (Clarendon Press, 1958).

[15] L. E. Cross, Journal of Materials Science **41**, 1573 (2006).

[16] P. V. Yudin and A. K. Tagantsev, Nanotechnology **24**, 432001, 432001 (2013).

[17] P. Zubko, G. Catalan, and A. K. Tagantsev, Annual Review of Materials Research **43**, 387 (2013).

[18] P. Koirala, C. A. Mizzi, and L. D. Marks, Nano Letters **18**, 3850 (2018).

[19] D. Lee, A. Yoon, S. Y. Jang, J. G. Yoon, J. S. Chung, M. Kim, J. F. Scott, and T. W. Noh, Physical Review Letters **107**, 057602, 057602 (2011).

[20] M. Gharbi, Z. H. Sun, P. Sharma, and K. White, Applied Physics Letters **95** (2009).

[21] C. R. Robinson, K. W. White, and P. Sharma, Applied Physics Letters **101** (2012).

[22] A. Abdollahi, C. Peco, D. Millan, M. Arroyo, G. Catalan, and I. Arias, Physical Review B **92**, 094101 (2015).

[23] S. Das, B. Wang, T. R. Paudel, S. M. Park, E. Y. Tsymbal, L. Q. Chen, D. Lee, and T. W. Noh, Nature Communications **10**, 537 (2019).

[24] T. A. L. Burgo, C. A. Silva, L. B. S. Balestrin, and F. Galembeck, Scientific Reports **3**, 8, 2384 (2013).

[25] K. Sayfidinov, S. D. Cezan, B. Baytekin, and H. T. Baytekin, Science Advances **4**, 6, eaau3808 (2018).

[26] K. Nakayama, Wear **194**, 185 (1996).

[27] M. Wolloch, G. Levita, P. Restuccia, and M. C. Righi, Physical Review Letters **121**, 026804 (2018).

[28] H. Hertz, Journal fur die Reine und Angewandte Mathematik **1882**, 156 (1882).

[29] K. L. Johnson, K. Kendall, and A. D. Roberts, Proceedings of the Royal Society of London Series a-Mathematical and Physical Sciences **324**, 301 (1971).

[30] T. A. Burgo and A. Erdemir, Angew Chem Int Ed Engl **53**, 12101 (2014).

[31] J. V. Escobar, A. Chakravarty, and S. J. Putterman, Diamond and Related Materials **36**, 8 (2013).

[32] K. M. Forward, D. J. Lacks, and R. M. Sankaran, Physical Review Letters **102**, 028001 (2009).

[33] R. Pham, R. C. Virnelson, R. M. Sankaran, and D. J. Lacks, Journal of Electrostatics **69**, 456 (2011).

[34] T. Shinbrot, T. S. Komatsu, and Q. Zhao, EPL (Europhysics Letters) **83**, 24004 (2008).

[35] S. R. Waitukaitis, V. Lee, J. M. Pierson, S. L. Forman, and H. M. Jaeger, Physical Review Letters **112**, 218001 (2014).

[36] H. T. Baytekin, A. Z. Patashinski, M. Branicki, B. Baytekin, S. Soh, and B. A. Gryzbowski, Science **333** (2011).

[37] T. A. Burgo, T. R. Ducati, K. R. Francisco, K. J. Clinckspoor, F. Galembeck, and S. E. Galembeck, Langmuir **28**, 7407 (2012).

[38] J. Hong and D. Vanderbilt, Physical Review B **88**, 174107 (2013).

[39] R. Resta, Physical Review Letters **105**, 127601 (2010).

[40] M. Stengel, Physical Review B **93**, 245107 (2016).

[41] C. E. Dreyer, M. Stengel, and D. Vanderbilt, Physical Review B **98**, 075153 (2018).

[42] S. M. Kogan, Soviet Physics-Solid State **5**, 2069 (1964).

[43] U. G. Musa, S. D. Cezan, B. Baytekin, and H. T. Baytekin, Scientific Reports **8**, 2472 (2018).

[44] B. D. Terris, J. E. Stern, D. Rugar, and H. J. Mamin, Physical Review Letters **63**, 2669 (1989).

[45] C. Xu *et al.*, ACS Nano **13**, 2034 (2019).

[46] E. Nemeth, V. Albrecht, G. Schubert, and F. Simon, Journal of Electrostatics **58**, 3 (2003).

[47] F.-R. Fan, L. Lin, G. Zhu, W. Wu, R. Zhang, and Z. L. Wang, Nano Letters **12**, 3109 (2012).

[48] G. Zhu, C. Pan, W. Guo, C. Y. Chen, Y. Zhou, R. Yu, and Z. L. Wang, Nano Letters **12**, 4960 (2012).

[49] R. D. I. G. Dharmasena, K. D. G. I. Jayawardena, C. A. Mills, J. H. B. Deane, J. V. Anguita, R. A. Dorey, and S. R. P. Silva, Energy and Environmental Science **10**, 1801 (2017).

[50] S. Niu, S. Wang, L. Lin, Y. Liu, Y. S. Zhou, Y. Hu, and Z. L. Wang, Energy and Environmental Science **6**, 3576 (2013).

[51] K. J. Wahl, D. N. Dunn, and I. L. Singer, Wear **230**, 175 (1999).

[52] A. G. Petrov, Biochim Biophys Acta **1561**, 1, Pii s0304-4157(01)00007-7 (2002).

[53] A. J. Walton, Advances in Physics **26**, 887 (1977).

[54] J. I. Zink, Accounts of Chemical Research **11**, 289 (1978).

[55] C. G. Camara, J. V. Escobar, J. R. Hird, and S. J. Putterman, Nature **455**, 1089 (2008).

[56] K. Nakayama and R. A. Nevshupa, Journal of Physics D: Applied Physics **35**, L53 (2002).

[57] See Supplemental Material at [URL will be inserted by publisher] for background information on flexoelectricity, triboelectricity, and tribology, and a detailed derivation and analysis of the model used in this work. The Supplemental Material includes Refs. [58-91].

[58] E. V. Bursian and O. I. Zaikovskii, Soviet Physics - Solid State **10**, 1121 (1968).

[59] R. B. Meyer, Physical Review Letters **22**, 918 (1969).

[60] J. Narvaez, F. Vasquez-Sancho, and G. Catalan, Nature **538**, 219 (2016).

[61] P. Zubko, G. Catalan, A. Buckley, P. R. L. Welche, and J. F. Scott, Physical Review Letters **99**, 167601 (2007).

[62] W. Ma and L. E. Cross, Applied Physics Letters **78**, 2920 (2001).

[63] A. Biancoli, C. M. Fancher, J. L. Jones, and D. Damjanovic, Nature Materials **14**, 224 (2015).

[64] M. Stengel, Nature Communications **4**, 2693 (2013).

[65] A. K. Tagantsev, Physical Review B **34**, 5883 (1986).

[66] J. Hong, G. Catalan, J. F. Scott, and E. Artacho, Journal of Physiscs: Condensed Matter **22**, 112201 (2010).

[67] R. Maranganti and P. Sharma, Physical Review B **80**, 054109 (2009).

[68] A. Abdollahi, F. Vasquez-Sancho, and G. Catalan, Physical Review Letters **121** (2018).

[69] J. Narvaez, S. Saremi, J. Hong, M. Stengel, and G. Catalan, Physical Review Letters **115**, 037601 (2015).

[70] L. Shu *et al.*, Applied Physics Letters **111**, 162901 (2017).

[71] B. Chu and D. R. Salem, Applied Physics Letters **101**, 103905 (2012).

[72] J. Liu, Y. Zhou, X. Hu, and B. Chu, Applied Physics Letters **112**, 232901 (2018).

[73] M. Marvan and A. Havranek, Progress in Colloid & Polymer Science **78**, 33 (1988).

[74] Y. Liao and L. Marks, International Materials Reviews **62**, 99 (2017).

[75] I. Altfeder and J. Krim, Journal of Applied Physics **111**, 6, 094916 (2012).

[76] A. P. Merkle and L. D. Marks, Philosophical Magazine Letters **87**, 527 (2007).

[77] A. P. Merkle and L. D. Marks, Tribology Letters **26**, 73 (2007).

[78] A. M'ndange-Pfupfu and L. D. Marks, Tribology Letters **47**, 431 (2012).

[79] A. M'Ndange-Pfupfu and L. D. Marks, Tribology Letters **39**, 163 (2010).

[80] K. Tian, N. N. Gosvami, D. L. Goldsby, Y. Liu, I. Szlufarska, and R. W. Carpick, Physical Review Letters **118**, 076103, 076103 (2017).

[81] K. Tian, D. L. Goldsby, and R. W. Carpick, Physical Review Letters **120**, 186101, 186101 (2018).

[82] K. L. Johnson, *Contact Mechanics* (Cambridge University Press, Cambridge, 1985).

[83] B. V. Derjaguin, V. M. Muller, and Y. P. Toporov, Journal of Colloid and Interface Science **53**, 314 (1975).

[84] D. Tabor, Journal of Colloid and Interface Science **58**, 2 (1977).

[85] A. K. Tagantsev and P. V. Yudin, *Flexoelectricity in Solids: From Theory to Applications* (WSPC, 2016).

[86] M. Stengel, Physical Review B **90**, 201112(R) (2014).

[87] A. K. Tagantsev and A. S. Yurkov, Journal of Applied Physics **112**, 044103 (2012).

[88] A. N. Morozovska, E. A. Eliseev, M. D. Glinchuk, L. Q. Chen, and V. Gopalan, Physical Review B **85**, 094107 (2012).

[89] Y. Cao, A. Morozovska, and S. V. Kalinin, Physical Review B **96**, 184109 (2017).

[90] A. N. Morozovska, E. A. Eliseev, A. K. Tagantsev, S. L. Bravina, L. Q. Chen, and S. V. Kalinin, Physical Review B **83**, 195313 (2011).

[91] J. E. Guyer, W. J. Boettinger, J. A. Warren, and G. B. McFadden, Physical Review E **69**, 021603 (2004).